Optimization-Based Collision Avoidance

Xiaojing Zhang*[a], Alexander Liniger*[b], Francesco Borrelli[a]

[a]*Model Predictive Control Laboratory, Department of Mechanical Engineering, University of California, Berkeley, USA*
[b]*Automatic Control Laboratory, Department of Information Technology and Electrical Engineering, ETH Zurich, Switzerland*

Abstract

This paper presents a novel method for reformulating non-differentiable collision avoidance constraints into *smooth* nonlinear constraints using strong duality of convex optimization. We focus on a controlled object whose goal is to avoid obstacles while moving in an n-dimensional space. The proposed reformulation does not introduce approximations, and applies to general obstacles and controlled objects that can be represented in an n-dimensional space as the finite union of convex sets. Furthermore, we connect our results with the notion of signed distance, which is widely used in traditional trajectory generation algorithms. Our method can be used in generic navigation and trajectory planning tasks, and the smoothness property allows the use of general-purpose gradient- and Hessian-based optimization algorithms. Finally, in case a collision cannot be avoided, our framework allows us to find "least-intrusive" trajectories, measured in terms of penetration. We demonstrate the efficacy of our framework on a quadcopter navigation and automated parking problem, and our numerical experiments suggest that the proposed methods enable real-time optimization-based trajectory planning problems in tight environments.

Keywords: obstacle avoidance, collision avoidance, path planning, autonomous parking, trajectory planning, navigation in tight environments

1. Introduction

Maneuvering autonomous systems in an environment with obstacles is a challenging problem that arises in a number of practical applications including robotic manipulators and trajectory planning for autonomous systems such as self-driving cars and quadcopters. In almost all of those applications, a fundamental feature is the system's ability to avoid collision with obstacles which are, for example, humans operating in the same area, other autonomous systems, or static objects such as walls.

Optimization-based trajectory planning algorithms such as Model Predictive Control (MPC) have received significant attention recently, ranging from (unmanned) aircraft to robots to autonomous cars [1, 2, 3,

[☆]E-mail addresses: {xiaojing.zhang, fborrelli}@berkeley.edu, liniger@control.ee.ethz.ch

4, 5, 6, 7, 8, 9, 10, 11, 12]. This can be attributed to the increase in computational resources, the availability of robust numerical algorithms for solving optimization problems, as well as MPC's ability to systematically encode system dynamics and constraints inside its formulation. This is in contrast to many sampling-based trajectory planning algorithms such as the rapidly expanding random tree (RRT), where convergence can be slow at times, and the generated trajectories far from optimal. Even though RRT* solves the latter problem and is able to find the optimal solution asymptotically, this comes at increased computational complexity, and faces scalability challenges for high dimensional systems. We refer the interested reader to the survey papers [13, 14] for a comprehensive review on existing trajectory planning and obstacle avoidance algorithms.

One fundamental challenge in optimization-based trajectory planning is the appropriate formulation of collision avoidance constraints, which are known to be non-convex and computationally difficult to handle in general. While a number of formulations have been proposed for collision avoidance constraints, they are typically limited by one of the following features: (*i*) The collision avoidance constraints are approximated through linear constraint, and it is difficult to establish the approximation error [9]; (*ii*) Existing formulations focus on point-mass controlled objects, and are not applicable to full-dimensional objects; (*iii*) When the obstacles are polyhedral, then the collision avoidance constraints are often reformulated using integer variables [15]. While this reformulation is attractive for linear systems with convex constraints since in this case a mixed-integer convex optimization problem can be solved, integer variables should generally be avoided when dealing with nonlinear systems when designing real-time controllers for robotic systems.

In this paper, we focus on a *controlled object* that moves in a general n-dimensional space while avoiding obstacles, and propose a novel approach for modeling obstacle avoidance constraints that overcomes the aforementioned limitations. Specifically, the contributions of this paper can be summarized as follows:

- We show that if the controlled object and the obstacles are described by convex sets such as polytopes or ellipsoids (or can be decomposed into a finite union of such convex sets), then the collision avoidance constraints can be exactly and non-conservatively reformulated as a set of smooth non-convex constraints. This is achieved by appropriately reformulating the *distance*-function between two convex sets using strong duality of convex optimization.

- We provide a second formulation for collision avoidance based on the notion of *signed distance*, which characterizes not only the distance between two objects but also their penetration. This reformulation allows us to compute "least-intrusive" trajectories in case collisions cannot be avoided. Numerical studies indicate that, compared to the first reformulation, this reformulation has the additional benefit of increased numerical stability when it comes to solving the (non-convex) optimization problems.

- Both our formulations allows the incorporation of system dynamics and input limits in the form of constraints. As a result, the trajectories generated from our obstacle avoidance algorithms are *kinodynamically feasible*, and can be easily tracked by some low-level controller.

- We demonstrate the efficacy of the proposed obstacle avoidance reformulations on a quadcopter trajectory planning problem and autonomous parking application, where the controlled vehicles must navigate in tight environments. We show that while the distance reformulation is generally computationally more efficient than the signed-distance approach, the latter is numerically more stable and able to find solutions even in challenging circumstances.

This paper is organized as follows: Section 2 introduces the problem setup. Section 3 presents the collision avoidance constraint reformulation for the special case when the controlled object is a point mass. The results are then extended to full-dimensional controlled objects in Section 4. Numerical experiments demonstrating the efficacy of the proposed method are given in Sections 5 and 6, and conclusions are drawn in Section 7. The Appendix contains auxiliary results needed to prove the main results of the paper.

Related Work

A large body of work exists on the topic of obstacle avoidance. In the following, we review optimization-based approaches, and refer the interested reader to [13, 14] for a comprehensive overview of the entire field. Broadly speaking, optimization-based collision-avoidance algorithms can be divided into two cases based on the modeling of the controlled object: point-mass models and full-dimensional objects. Due to its conceptual simplicity, the vast majority of literature focuses on collision avoidance for point-mass models, and consider the shape of the controlled object by inflating the obstacles. The obstacles are generally assumed to be either polytopes or ellipsoids. For polyhedral obstacles, disjunctive programming can be used to ensure collision avoidance, which is often reformulated as a mixed-integer optimization problem [1, 4, 15]. In case of ellipsoidal obstacles, the collision avoidance constraints can be formulated as a smooth non-convex constraint [16, 17, 18], and the resulting optimization problem can be solved using generic non-linear programming solvers.

The case of full-dimensional controlled objects has, to be best of the author's knowledge, not been widely studied in the context of optimization-based methods, with the exception of [9, 19]. In [19], the authors model the controlled object through its vertices and, under the assumption that all involved object are rectangles, ensure collision avoidance by keeping all vertices of the controlled object outside the obstacle. A more general way of handling collision avoidance for full-dimensional controlled object has been proposed in [9] by using the notion of signed distance. Unfortunately, it is generally difficult to obtain an explicit representation of the signed distance; as a result, it is typically linearized or approximated by employing sequential optimization techniques [9].

The approach most closely related to our formulation is probably the work of [6], where the authors propose a smooth reformulation of the collision avoidance constraint for point-mass controlled objects and polyhedral obstacles. However, our approach differs from [6] as (i) our approach easily generalizes to full-dimensional controlled objects, and (ii) we are, based on the notion of penetration, also able to compute least-intrusive trajectories in case collisions cannot be avoided.

Notation

Given a proper cone $\mathcal{K} \subset \mathbb{R}^l$ and two vectors $a, b \in \mathbb{R}^l$, then $a \preceq_{\mathcal{K}} b$ is equivalent to $(b - a) \in \mathcal{K}$. Furthermore, if $\mathcal{K} = \mathbb{R}^l_+$ is the standard cone, then $\preceq_{\mathbb{R}^l_+}$ denotes element-wise inequality, and we write $\leq$ instead. Moreover, $\|\cdot\|_*$ is the dual norm of $\|\cdot\|$, and $\mathcal{K}^* \subset \mathbb{R}^l$ is the dual cone of $\mathcal{K}$. The "space" occupied by the controlled object (e.g., a drone, vehicle, or robot in general) is denoted as $\mathbb{E} \subset \mathbb{R}^n$; similarly, the space occupied by the obstacles is denoted as $\mathbb{O} \subset \mathbb{R}^n$.

2. Problem Description

2.1. Dynamics, Objective and Constraints

We assume that the dynamics of the controlled object takes the form

$$x_{k+1} = f(x_k, u_k), \tag{1}$$

where $x_k \in \mathbb{R}^{n_x}$ is the state of the controlled object at time step k given an initial state $x_0 = x_S$, $u_k \in \mathbb{R}^{n_u}$ is the control input, and $f\colon \mathbb{R}^{n_x} \times \mathbb{R}^{n_u} \to \mathbb{R}^{n_x}$ describes the dynamics of the system. In most cases, the state x_k contains information such as the position $p_k \in \mathbb{R}^n$ and angles $\theta_k \in \mathbb{R}^n$ of the controlled object, as well the velocities $\dot{p}_k$ and angular rates $\dot{\theta}_k$. In this paper, we assume that no disturbance is present, and that the system is subject to input and state constraints of the form

$$h(x_k, u_k) \leq 0, \tag{2}$$

where $h : \mathbb{R}^{n_x} \times \mathbb{R}^{n_u} \to \mathbb{R}^{n_h}$, n_h is the number of constraints, and the inequality in (2) is interpreted element-wise. Our goal is to find a control sequence, over a horizon N, which allows the controlled object to navigate from the initial state x_S to its final state $x_F \in \mathbb{R}^{n_x}$, while optimizing some objective function $J = \sum_{k=0}^{N} \ell(x_k, u_k)$, where $\ell\colon \mathbb{R}^{n_x} \times \mathbb{R}^{n_u} \to \mathbb{R}$ is a stage cost, and avoiding $M \geq 1$ obstacles $\mathbb{O}^{(1)}, \mathbb{O}^{(2)}, \ldots, \mathbb{O}^{(M)} \subset \mathbb{R}^n$. Throughout this paper, we assume that the functions $f(\cdot,\cdot)$, $h(\cdot,\cdot)$ and $\ell(\cdot,\cdot)$ are smooth. Smoothness is assumed for simplicity, although all forthcoming results apply equally to cases when those functions are twice continuously differentiable.

2.2. Obstacle and Controlled Object Modeling

Given the state x_k, we denote by $\mathbb{E}(x_k) \subset \mathbb{R}^n$ the "space" occupied by the controlled object at time k, which we assume is a subset of $\mathbb{R}^n$. The collision avoidance constraint at time k is now given by[1].

$$\mathbb{E}(x_k) \cap \mathbb{O}^{(m)} = \emptyset, \quad \forall m = 1, \ldots, M. \tag{3}$$

Constraint (3) is non-differentiable in general, e.g., when the obstacles are polytopic [6, 9]. In this paper, we will remodel (3) in such a way that both continuity and differentiability are preserved. To this end, we assume that the obstacles $\mathbb{O}^{(m)}$ are convex compact sets with non-empty relative interior[2], and can be represented as

$$\mathbb{O}^{(m)} = \{y \in \mathbb{R}^n \colon A^{(m)} y \preceq_{\mathcal{K}} b^{(m)}\}, \tag{4}$$

where $A^{(m)} \in \mathbb{R}^{l \times n}$, $b^{(m)} \in \mathbb{R}^l$, and $\mathcal{K} \subset \mathbb{R}^l$ is a closed convex pointed cone with non-empty interior. Representation (4) is entirely generic since any compact convex set admits a conic representation of the form (4) [20, p.15]. In particular, polyhedral obstacles can be represented as (4) by choosing $\mathcal{K} = \mathbb{R}^l_+$; in this case $\preceq_{\mathcal{K}}$ corresponds to the well-known element-wise inequality $\leq$. Likewise, ellipsoidal obstacles can be represented by letting $\mathcal{K}$ be the second-order cone, see [21]. To simplify the upcoming exposition, the same cone $\mathcal{K}$ is assumed for all obstacles; the extension to obstacle-specific cones $\mathcal{K}^{(m)}$ is straight-forward.

In this paper, we will consider controlled objects $\mathbb{E}(x_k)$ that are modeled as *point-masses* as well as *full-dimensional* objects. In the former case, $\mathbb{E}(x_k)$ simply extracts the position p_k from the state x_k, i.e.,

$$\mathbb{E}(x_k) = p_k. \tag{5a}$$

In the latter case, we will model the controlled object $\mathbb{E}(x_k)$ as the rotation and translation of an "initial" convex set $\mathbb{B} \subset \mathbb{R}^n$, i.e.,

$$\mathbb{E}(x_k) = R(x_k)\mathbb{B} + t(x_k), \quad \mathbb{B} := \{y \colon Gy \preceq_{\bar{\mathcal{K}}} g\}, \tag{5b}$$

where $R \colon \mathbb{R}^{n_x} \to \mathbb{R}^{n \times n}$ is an (orthogonal) rotation matrix and $t \colon \mathbb{R}^{n_x} \to \mathbb{R}^n$ is the translation vector. The matrices $(G, g) \in \mathbb{R}^{h \times n} \times \mathbb{R}^h$ and the cone $\bar{\mathcal{K}}$, which we assume is closed, convex and pointed, define the shape of our initial (compact) set $\mathbb{B}$. Often, the rotation matrix $R(\cdot)$ depends on the angles θ_k of the controlled object, while the translation vector $t(\cdot)$ depends on the position p_k of the controlled object. We assume throughout that the functions $R(\cdot)$ and $t(\cdot)$ are smooth.

[1]In this paper, we only consider collision avoidance constraints that are associated with the position and geometric shape of the controlled object, which are typically defined by its position p_k and angles θ_k. This is not a restriction of the theory as the forthcoming approaches can be easily generalized to collision avoidance involving other states, but done to simplify exposition of the material.

[2]Non-convex obstacles can often be approximated/decomposed as the union of convex obstacles

2.3. Optimal Control Problem with Collision Avoidance

By combining (1)–(3), the constrained finite-horizon optimal control problem with collision avoidance constraint is given by

$$\begin{aligned}\min_{\mathbf{x},\mathbf{u}} \quad & \sum_{k=0}^{N} \ell(x_k,u_k) \\ \text{s.t.} \quad & x_0 = x_S,\ x_{N+1} = x_F \\ & \left.\begin{aligned} & x_{k+1} = f(x_k,u_k), \\ & h(x_k,u_k) \le 0, \\ & \mathbb{E}(x_k) \cap \mathbb{O}^{(m)} = \emptyset, \end{aligned}\right\} \begin{aligned} & k = 0,\dots,N, \\ & m = 1,\dots,M, \end{aligned}\end{aligned} \tag{6}$$

where $\mathbb{E}(x_k)$ is either given by (5a) (point-mass model) or (5b) (full-dimensional set), $\mathbf{x} := [x_0, x_1, \dots, x_{N+1}]$ is the collection of all states, and $\mathbf{u} := [u_0, u_1, \dots, u_N]$ is the collection of all inputs. A key difficulty in solving problem (6), even for linear systems with convex objective function and convex state/input constraints, is the presence of the collision-avoidance constraints $\mathbb{E}(x_k) \cap \mathbb{O}^{(m)} = \emptyset$, which in general are non-convex and non-differentiable [6, 9]. In the following, we present two novel approaches for modeling collision avoidance constraints that preserve continuity and differentiability, and are amendable for use with existing off-the-shelf gradient- and Hessian-based optimization algorithms.

2.4. Collision Avoidance

A popular way of formulating collision avoidance, which holds for generic sets $\mathbb{E}(x) \subset \mathbb{R}^n$ and $\mathbb{O} \subset \mathbb{R}^n$, is based on the *signed distance* [9]

$$\operatorname{sd}(\mathbb{E}(x),\mathbb{O}) := \operatorname{dist}(\mathbb{E}(x),\mathbb{O}) - \operatorname{pen}(\mathbb{E}(x),\mathbb{O}), \tag{7}$$

where $\operatorname{dist}(\cdot,\cdot)$ and $\operatorname{pen}(\cdot,\cdot)$ are the distance and penetration function, and are defined as

$$\operatorname{dist}(\mathbb{E}(x),\mathbb{O}) := \inf_t \{\|t\| \colon \mathbb{E}(x) + t \in \mathbb{O}\}, \tag{8a}$$

$$\operatorname{pen}(\mathbb{E}(x),\mathbb{O}) := \inf_t \{\|t\| \colon \mathbb{E}(x) + t \notin \mathbb{O}\}. \tag{8b}$$

For convex sets $\mathbb{E}(x)$ and $\mathbb{O}$, the signed distance is positive if $\mathbb{E}(x)$ and $\mathbb{O}$ do not intersect, zero if their intersection has empty interior, and negative if their intersection has non-empty interior. Therefore, collision avoidance can be ensured by requiring $\operatorname{sd}(\mathbb{E}(x),\mathbb{O}) > 0$. Unfortunately, directly enforcing $\operatorname{sd}(\mathbb{E}(x),\mathbb{O}) > 0$ inside the optimization problem (6) is generally difficult since it is non-convex and non-differentiable in general [9]. Furthermore, for optimization algorithms to be numerically efficient, they require an explicit representation of the functions they are dealing with, in this case $\operatorname{sd}(\cdot,\cdot)$. This, however, is difficult to obtain in practice since $\operatorname{sd}(\cdot,\cdot)$ itself is the solution of the optimization problems (8a) and (8b). As a result, existing algorithm approximate (7) through local linearization [9], for which it is difficult to establish bounds on approximation errors.

In the following, we propose two reformulation techniques for obstacles avoidance that overcome the issues of non-differentaibility and does not require an explicit representation of the signed distance. We begin with the case when the point-mass model in Section 3, and treat the general case of a full-dimensional controlled object in Section 4.

3. Collision Avoidance for Point-Mass Models

In this section, we first present a smooth reformulation for (6) when $\mathbb{E}(x_k) = p_k$ (Section 3.1), and then extend the approach in Section 3.2 to generate minimum-penetration trajectories in case collisions cannot be avoided. To simplify notation, the time indices k are omitted in the remainder of this section.

3.1. Collision-Free Trajectory Generation

Proposition 1. *Assume that the obstacle $\mathbb{O}$ and the controlled object are given as in* (4) *and* (5a)*, respectively, and let $\mathsf{d}_{\min} \geq 0$ be a desired safety margin between the controlled object and the obstacle. Then we have:*

$$\operatorname{dist}(\mathbb{E}(x), \mathbb{O}) > \mathsf{d}_{\min} \iff \exists \lambda \succeq_{\mathcal{K}^*} 0 \colon (A\,p - b)^\top \lambda > \mathsf{d}_{\min}, \ \|A^\top \lambda\|_* \leq 1. \tag{9}$$

Proof. It follows from (4) and (8a) that $\operatorname{dist}(\mathbb{E}(x), \mathbb{O}) = \min_t \{\|t\| \colon A(\mathbb{E}(x) + t) \preceq_{\mathcal{K}} b\}$. Following [21, p.401], its dual problem is given by $\max_\lambda \left\{(A\mathbb{E}(x) - b)^\top \lambda \colon \|A^\top \lambda\|_* \leq 1, \ \lambda \succeq_{\mathcal{K}^*} 0\right\}$, where $\|\cdot\|_*$ is the dual norm associated to $\|\cdot\|$ and $\mathcal{K}^*$ is the dual cone of $\mathcal{K}$. Since $\mathbb{O}$ is assumed to have non-empty relative interior, strong duality holds, and $\operatorname{dist}(\mathbb{E}(x), \mathbb{O}) = \max_\lambda \left\{(A\,\mathbb{E}(x) - b)^\top \lambda \colon \|A^\top \lambda\|_* \leq 1, \ \lambda \succeq_{\mathcal{K}^*} 0\right\}$. Hence, for any non-negative scalar $\mathsf{d}_{\min}$, $\operatorname{dist}(\mathbb{E}(x), \mathbb{O}) > \mathsf{d}_{\min}$ is satisfied if, and only if, there exists $\lambda \succeq_{\mathcal{K}^*} 0 \colon (A\,\mathbb{E}(x) - b)^\top \lambda > \mathsf{d}_{\min}, \ \|A^\top \lambda\|_* \leq 1$. The desired result follows from identity (5a). □

Intuitively speaking, any variable λ satisfying the right-hand-side of (9) is a certificate verifying the condition $\operatorname{dist}(\mathbb{E}(x), \mathbb{O}) > \mathsf{d}_{\min}$. Since $\mathbb{E}(x) \cap \mathbb{O} = \emptyset$ is equivalent to $\operatorname{dist}(\mathbb{E}(x), \mathbb{O}) > 0$, the optimal control problem (6) for the point-mass model (5a) is given by

$$\begin{aligned}
\min_{\mathbf{x},\mathbf{u},\boldsymbol{\lambda}} \quad & \sum_{k=0}^{N} \ell(x_k, u_k) \\
\text{s.t.} \quad & x_0 = x_S, \ x_{N+1} = x_F, \\
& \left.\begin{aligned}
& x_{k+1} = f(x_k, u_k), \ h(x_k, u_k) \leq 0, \\
& (A^{(m)} p_k - b^{(m)})^\top \lambda_k^{(m)} > 0, \\
& \|A^{(m)\top} \lambda_k^{(m)}\|_* \leq 1, \ \lambda_k^{(m)} \succeq_{\mathcal{K}^*} 0
\end{aligned}\right\} \begin{aligned} & k = 0, \ldots, N, \\ & m = 1, \ldots, M, \end{aligned}
\end{aligned} \tag{10}$$

where p_k is the position of the controlled object at time k, $\lambda_k^{(m)}$ is the dual variable associated with obstacle $\mathbb{O}^{(m)}$ at time step k, and the optimization is performed over the states $\mathbf{x}$, the inputs $\mathbf{u}$ and the dual variables

$\boldsymbol{\lambda} = [\lambda_0^{(1)}, \ldots, \lambda_0^{(m)}, \lambda_1^{(1)}, \ldots, \lambda_N^{(m)}]$. We emphasize that (10) is an *exact* reformulation of (6) and that the optimal trajectory $\mathbf{x}^* = [x_0^*, x_1^*, \ldots, x_N^*]$ obtained by solving (6) is *kinodynamically feasible*.

Remark 1. Without further assumptions on the norm $\|\cdot\|$ and the cone $\mathcal{K}$, the last two constraints in (10) are not guaranteed to be smooth, a property that many general-purpose non-linear optimization algorithms require[3]. Fortunately, it turns out that these constraints are smooth for the practically relevant cases of $\|\cdot\|$ being the Euclidean distance and $\mathcal{K}$ either the standard cone or the second-order cone, which allows us to model polyhedral and ellipsoidal obstacles. In these case, and under the assumption that the functions $f(\cdot,\cdot)$, $h(\cdot,\cdot)$ and $\ell(\cdot,\cdot)$ are smooth, (10) is a smooth nonlinear optimization problem that is amendable to general-purpose non-linear optimization algorithms such as IPOPT [22]. Without going into details, we point out that smoothness is retained when $\|\cdot\| = \|\cdot\|_p$ is a general p-norm, with $p \in (1, \infty)$, and $\mathcal{K}$ is the cartesian product of p-order cones $\mathcal{K}_p := \{(s, z) \colon \|z\|_p \leq s\}$, with $p \in (1, \infty)$.

While reformulation (10) can be used for obstacle avoidance, it is limited to finding collision-free trajectories. In case collisions cannot be avoided, however, the above formulation is not able to find "least-intrusive" trajectories. Intuitively speaking, this is because (10) is based on the notion of distance, and the distance between two overlapping objects (as is in the case of collision), is always zero. From a practical point of view, this implies that slack variables cannot be included in the constraints of (9), because the optimal control problem is not able to distinguish between "severe" and "less severe" colliding trajectories. Finally, we point out that in practice, it is always desirable to include slack variables since (local) infeasibilities in non-convex optimization problem are known to cause severe numerical difficulties. In the following, we show how this limitation can be overcome by considering the notion of penetration.

3.2. Minimum-Penetration Trajectory Generation

In this section, we consider the design of *minimum-penetration* trajectories for cases when collision cannot be avoided and the goal is to find a "least-intrusive" trajectory. Following the literature [23, 24], we measure "intrusion" in terms of *penetration* as defined in (8b).

Proposition 2. *Assume that the obstacle* $\mathbb{O}$ *and controlled object are given as in* (4) *and* (5a)*, respectively, and let* $\mathsf{p}_{\max} \geq 0$ *be a desired maximum penetration of the controlled object and the obstacle. Then we have:*

$$\operatorname{pen}(\mathbb{E}(x), \mathbb{O}) < \mathsf{p}_{\max} \iff \exists \lambda \succeq_{\mathcal{K}^*} 0 \colon (b - Ap)^\top \lambda < \mathsf{p}_{\max}, \ \|A^\top \lambda\|_* = 1. \tag{11}$$

Proof. The proof, along with auxiliary lemmas, is given in Appendix A. □

[3] Strictly speaking, these solvers often require the cost function and constraints to be twice continuously differentiable only. Smoothness is assumed in this paper for the sake of simplicity.

Proposition 2 resembles Proposition 1 with the difference that the convex inequality constraint $\|A^\top \lambda\|_* \leq 1$ is replaced with the non-convex equality constraint $\|A^\top \lambda\|_* = 1$. In the following, we will see that Propositions 1 and 2 can be combined to represent the *signed distance* as defined in (7).

Theorem 1. *Assume that the obstacle $\mathbb{O}$ and the controlled object are given as in* (4) *and* (5a)*, respectively. Then, for any $\mathsf{d} \in \mathbb{R}$, we have:*

$$\mathrm{sd}(\mathbb{E}(x), \mathbb{O}) > \mathsf{d} \iff \exists \lambda \succeq_{\mathcal{K}^*} 0\colon (A\,p - b)^\top \lambda > \mathsf{d},\ \|A^\top \lambda\|_* = 1. \tag{12}$$

Proof. By definition, $\mathrm{sd}(\mathbb{E}(x), \mathbb{O}) = \mathrm{dist}(\mathbb{E}(x), \mathbb{O})$ if $\mathbb{E}(x) \cap \mathbb{O} = \emptyset$, and $\mathrm{sd}(\mathbb{E}(x), \mathbb{O}) = -\mathrm{pen}(\mathbb{E}(x), \mathbb{O})$ if $\mathbb{E}(x) \cap \mathbb{O} \neq \emptyset$. Let $\mathbb{E}(x) \cap \mathbb{O} \neq \emptyset$, in which case (12) follows directly from (11). If $\mathbb{E}(x) \cap \mathbb{O} = \emptyset$, then we have from (9) that $\mathrm{sd}(\mathbb{E}(x), \mathbb{O}) > \mathsf{d}$ is equivalent to $\exists \lambda \succeq_{\mathcal{K}^*} 0\colon (A\,p - b)^\top \lambda > \mathsf{d},\ \|A^\top \lambda\|_* \leq 1$. Due to homogeneity with respect to λ, if the previous condition is satisfied, then there always exists another dual multiplier $\lambda' \succeq_{\mathcal{K}^*} 0$ such that $(A\,p - b)^\top \lambda' > \mathsf{d},\ \|A^\top \lambda'\|_* = 1$. This concludes the proof. □

Reformulation (12) is similar to reformulation (9), with the difference that (12) holds for all $\mathsf{d} \in \mathbb{R}$, while (9) only holds for $\mathsf{d} \geq 0$. The "price" we pay for this generalization is that the convex constraint $\|A^\top \lambda\|_* \leq 1$ is turned into the non-convex equality constraint $\|A^\top \lambda\|_* = 1$ which, as we will see later on, generally results in longer compuation times. Nevertheless, Theorem 1 allows us to compute trajectories of least penetration whenever collision cannot be avoided by solving the following soft-constrained *minimum-penetration* problem:

$$\begin{aligned}
\min_{\mathbf{x},\mathbf{u},\mathbf{s},\boldsymbol{\lambda}} \quad & \sum_{k=0}^{N} \left[\ell(x_k, u_k) + \kappa \cdot \sum_{m=1}^{M} s_k^{(m)} \right] \\
\text{s.t.} \quad & x_0 = x(0),\ x_{N+1} = x_F, \\
& \left.\begin{aligned}
& x_{k+1} = f(x_k, u_k),\ h(x_k, u_k) \leq 0, \\
& (A^{(m)} p_k - b^{(m)})^\top \lambda_k^{(m)} > -s_k^{(m)}, \\
& \|A^{(m)\top} \lambda_k^{(m)}\|_* = 1,\ s_k^{(m)} \geq 0,\ \lambda_k^{(m)} \succeq_{\mathcal{K}^*} 0
\end{aligned}\right\} \begin{aligned} & k = 0, \ldots, N, \\ & m = 1, \ldots, M \end{aligned}
\end{aligned} \tag{13}$$

where p_k is the position of the controlled object at time k, $s_k^{(m)} \in \mathbb{R}_+$ is the slack variable associated to the object $\mathbb{O}^{(m)}$ at time step k, and $\kappa \geq 0$ is a weight factor that keeps the slack variable as close to zero as possible. Without going into details, we point out that the weight κ should be chosen "big enough" such that the slack variables only become active when the original problem is infeasible, i.e., when obstacle avoidance is not possible [25]. Notice that a positive slack variable implies a colliding trajectory, where the penetration depth is given by $s_k^{(m)}$. We close this section by pointing out that if, a priori, it is known that a collision-free trajectory can be generated, then formulation (10) should be given preference over formulation (13) because the former has fewer decision variables, and because the constraint $\|A^{(m)\top} \lambda_k^{(m)}\|_* \leq 1$ is convex, which generally leads to improved solution times. Smoothness of (13) is ensured if $\|\cdot\|$ is the Euclidean distance, and $\mathcal{K}$ is either the standard cone or the second-order cone, see Remark 1 for details.

4. Collision Avoidance for Full-Dimension Controlled Objects

In the previous section, we provided a framework for generating collision-free and minimum-penetration trajectories for controlled objects that are described by point-mass models. While such models can be used to generate trajectories for "ball-shaped" controlled objects, done by setting the minimum distance $d_{\min}$ equal to the radius of the controlled object (see Section 5 for such an example), it can be restrictive in other cases. For example, modeling a car in a parking lot as a Euclidean ball is generally a crude approximation, and might prevent the car from finding a parking spot. To alleviate this issue, we show in this section how the results of Section 3 can be extended to full-dimensional controlled objects.

4.1. Collision-Free Trajectory Generation

Similar to Section 3, we begin by first reformulating the distance function, which will allow us to generate collision-free trajectories:

Proposition 3. *Assume that the controlled object and the obstacle are given as in* (5b) *and* (4)*, respectively, and let* $\mathsf{d}_{\min} \geq 0$ *be a desired safety margin. Then we have:*

$$\begin{aligned}&\operatorname{dist}(\mathbb{E}(x), \mathbb{O}) > \mathsf{d}_{\min}\\ &\quad\iff \exists \lambda \succeq_{\mathcal{K}^*} 0, \mu \succeq_{\bar{\mathcal{K}}^*} 0\colon\ -g^\top \mu + (At(x) - b)^\top \lambda > \mathsf{d}_{\min},\ G^\top \mu + R(x)^\top A^\top \lambda = 0,\ \|A^\top \lambda\|_* \leq 1.\end{aligned} \tag{14}$$

Proof. Recall that $\operatorname{dist}(\mathbb{E}(x), \mathbb{O}) = \min_{e,o}\{\|e-o\| \colon Ao \preceq_{\mathcal{K}} b, e \in \mathbb{E}(x)\} = \min_{e',o}\{\|R(x)e' + t(x) - o\| \colon Ao \preceq_{\mathcal{K}} b, Ge' \preceq_{\bar{\mathcal{K}}} g\}$, where the last equality follows from (5b). The dual of this minimization problem is given by $\max_{\lambda,\mu}\{-g^\top \mu + (At(x) - b)^\top \lambda \colon G^\top \mu + R(x)^\top A^\top \lambda = 0,\ \|A^\top \lambda\|_* \leq 1,\ \lambda \succeq_{\mathcal{K}^*} 0,\ \mu \succeq_{\bar{\mathcal{K}}^\star} 0\}$, see e.g., [21, Section 8.2] for the derivation, where $\|\cdot\|_*$ is the dual norm, and $\mathcal{K}^*$ and $\bar{\mathcal{K}}^\star$ are the dual cones of $\mathcal{K}$ and $\bar{\mathcal{K}}$, respectively. Since $\mathbb{O}$ and $\mathbb{B}$ are assumed to have non-empty relative interior, strong duality holds, and $\operatorname{dist}(\mathbb{E}(x), \mathbb{O}) > \mathsf{d}_{\min} \Leftrightarrow \max_{\lambda,\mu}\{-g^\top \mu + (At(x) - b)^\top \lambda \colon G^\top \mu + R(x)^\top A^\top \lambda = 0,\ \|A^\top \lambda\|_* \leq 1,\ \lambda \succeq_{\mathcal{K}^*} 0,\ \mu \succeq_{\bar{\mathcal{K}}^\star} 0\} > \mathsf{d}_{\min} \Leftrightarrow \exists \lambda \succeq_{\mathcal{K}^*} 0, \mu \succeq_{\bar{\mathcal{K}}^*} 0\colon -g^\top \mu + (At(x) - b)^\top \lambda > \mathsf{d}_{\min},\ G^\top \mu + R(x)^\top A^\top \lambda = 0,\ \|A^\top \lambda\|_* \leq 1.$ □

Compared to Proposition 1, we see that full-dimensional controlled objects require the introduction of the additional dual variables $\mu^{(m)}$, one for each obstacle $\mathbb{O}^{(m)}$. By setting $\mathsf{d}_{\min} = 0$, we obtain now the following reformulation of (6) for full-dimensional objects:

$$\begin{aligned}\min_{\mathbf{x},\mathbf{u},\boldsymbol{\lambda},\boldsymbol{\mu}} \quad & \sum_{k=0}^{N} \ell(x_k, u_k)\\ \text{s.t.} \quad & x_0 = x(0),\ x_{N+1} = x_F,\\ & \left.\begin{aligned} & x_{k+1} = f(x_k, u_k),\ h(x_k, u_k) \leq 0,\\ & -g^\top \mu_k^{(m)} + (A^{(m)} t(x_k) - b^{(m)})^\top \lambda_k^{(m)} > 0,\\ & G^\top \mu_k^{(m)} + R(x_k)^\top {A^{(m)}}^\top \lambda_k^{(m)} = 0,\\ & \|{A^{(m)}}^\top \lambda_k^{(m)}\|_* \leq 1,\ \lambda_k^{(m)} \succeq_{\mathcal{K}^*} 0,\ \mu_k^{(m)} \succeq_{\bar{\mathcal{K}}^*} 0,\end{aligned}\right\} \begin{aligned}& k = 0, \ldots, N,\\ & m = 1, \ldots, M,\end{aligned}\end{aligned} \tag{15}$$

where $\lambda_k^{(m)}$ and $\mu_k^{(m)}$ are the dual variables associated with the obstacle $\mathbb{O}^{(m)}$ at step k, $\boldsymbol{\lambda}$ and $\boldsymbol{\mu}$ are the collection of all $\lambda_k^{(m)}$ and $\mu_k^{(m)}$, respectively, and the optimization is performed over $(\mathbf{x}, \mathbf{u}, \boldsymbol{\lambda}, \boldsymbol{\mu})$. Notice that (15) is an *exact* reformulation of (6). Smoothness of (15) is ensured if $\|\cdot\|$ is the Euclidean distance, and $\mathcal{K}$ and $\bar{\mathcal{K}}$ are either the standard cone or the second-order cone, see also Remark 1.

Similar to the point-mass case in Section 3.1, the optimal control problem (15) is able to generate collision-free trajectories, but unable to find "least-intrusive" trajectories in case collision-free trajectories cannot be found. This is addressed next.

4.2. Minimum-Penetration Trajectory Generation

We overcome the above limitation by considering once more the notion of penetration. We begin with the following result:

Proposition 4. *Assume that the obstacles and controlled object are given as in* (4) *and* (5b)*, respectively, and let* $\mathsf{p}_{\max} \geq 0$ *be a maximal penetration depth. Then we have:*

$$\begin{aligned} &\operatorname{pen}(\mathbb{E}(x), \mathbb{O}) < \mathsf{p}_{\max} \\ &\quad \iff \exists \lambda \succeq_{\mathcal{K}^*} 0, \mu \succeq_{\bar{\mathcal{K}}^*} 0\colon g^\top \mu + (b - A\,t(x))^\top \lambda < \mathsf{p}_{\max},\ G^\top \mu + R(x)^\top A^\top \lambda = 0,\ \|A^\top \lambda\|_* = 1. \end{aligned} \tag{16}$$

Proof. Notice that $\operatorname{pen}(\mathbb{E}(x), \mathbb{O}) = \operatorname{pen}(0, \mathbb{O} - \mathbb{E}(x))$, where $\mathbb{O} - \mathbb{E}(x) := \{o - e\colon o \in \mathbb{O},\ e \in \mathbb{E}(x)\}$ is the Minkowski difference [23]. Furthermore, it follows from the proof of Proposition 2 that $\operatorname{pen}(0, \mathbb{O} - \mathbb{E}(x)) = \inf_{\{z\colon \|z\|_*=1\}}\{\max_{y \in \mathbb{O} - \mathbb{E}(x)}\{y^\top z\}\}$. Using strong duality of convex optimization, we can dualize the inner maximization problem as $\max_{o \in \mathbb{O}, e \in \mathbb{E}(x)}\{z^\top (o - e)\} = \max_{o \in \mathbb{O}, e' \in \mathbb{B}}\{z^\top (o - R(x)e' - t(x))\} = \min_{\lambda,\mu}\{b^\top \lambda + g^\top \mu - z^\top t(x)\colon A^\top \lambda = z,\ G^\top \mu = -R^\top z\colon \lambda \succeq_{K^*} 0,\ \mu \succeq_{\bar{\mathcal{K}}^*} 0\}$. Hence, $\operatorname{pen}(0, \mathbb{O} - \mathbb{E}(x)) = \inf_{z,\lambda,\mu}\{b^\top \lambda + g^\top \mu - z^\top t(x)\colon A^\top \lambda = z,\ G^\top \mu = -R^\top z,\ \|z\|_* = 1\}$. Eliminating the z-variable using the first equality constraint and following the steps of the proof of Proposition 2 gives the desired result. □

Similar to the point-mass case, the reformulation of penetration differs from the reformulation of distance in that the (convex) inequality constraint $\|A^\top \lambda\|_* \leq 1$ becomes a non-convex equality constraint $\|A^\top \lambda\|_* = 1$. The following theorem shows that Propositions 3 and 4 can be combined to represent the *signed distance* function.

Theorem 2. *Assume that the obstacles and controlled object are given as in* (4) *and* (5b)*, respectively. Then, for any* $\mathsf{d} \in \mathbb{R}$*, we have:*

$$\begin{aligned} &\operatorname{sd}(\mathbb{E}(x), \mathbb{O}) > \mathsf{d} \\ &\quad \iff \exists \lambda \succeq_{\mathcal{K}^*} 0, \mu \succeq_{\bar{\mathcal{K}}^*} 0\colon -g^\top \mu + (At(x) - b)^\top \lambda > \mathsf{d},\ G^\top \mu + R(x)^\top A^\top \lambda = 0,\ \|A^\top \lambda\|_* = 1. \end{aligned} \tag{17}$$

Proof. By definition, $\operatorname{sd}(\mathbb{E}(x), \mathbb{O}) = \operatorname{dist}(\mathbb{E}(x), \mathbb{O})$ if $\mathbb{E}(x) \cap \mathbb{O} = \emptyset$, and $\operatorname{sd}(\mathbb{E}(x), \mathbb{O}) = -\operatorname{pen}(\mathbb{E}(x), \mathbb{O})$ if $\mathbb{E}(x) \cap \mathbb{O} \neq \emptyset$. Consider now $\mathbb{E}(x) \cap \mathbb{O} \neq \emptyset$, in which case (17) follows directly from (16). Assume now that $\mathbb{E}(x) \cap \mathbb{O} = \emptyset$; then we have from (14) that $\mathrm{sd}(\mathbb{E}(x), \mathbb{O}) > \mathsf{d}$ is equivalent to $\exists \lambda \succeq_{\mathcal{K}^*} 0, \mu \succeq_{\bar{\mathcal{K}}^*} 0\colon\ -g^\top \mu + (At(x) - b)^\top \lambda > \mathsf{d},\ G^\top \mu + R(x)^\top A^\top \lambda = 0,\ \|A^\top \lambda\|_* \leq 1$. Due to homogeneity with respect to λ and μ, if the previous condition is satisfied, then there also exists a $\lambda' \succeq_{\mathcal{K}^*} 0$ and $\mu' \succeq_{\bar{\mathcal{K}}^*} 0$ such that $-g^\top \mu + (At(x) - b)^\top \lambda > \mathsf{d},\ G^\top \mu + R(x)^\top A^\top \lambda = 0,\ \|A^\top \lambda\|_* = 1$. This concludes the proof. □

Theorem 2 now allows us to formulate the following soft-constrained *minimum-penetration* optimal control problem

$$\begin{aligned}
\min_{\mathbf{x},\mathbf{u},\mathbf{s},\boldsymbol{\lambda},\boldsymbol{\mu}} \quad & \sum_{k=0}^{N} \left[\ell(x_k, u_k) + \kappa \cdot \sum_{m=1}^{M} s_k^{(m)} \right] \\
\text{s.t.} \quad & x_0 = x_S,\ x_{N+1} = x_F, \\
& \left.\begin{aligned}
& x_{k+1} = f(x_k, u_k),\ h(x_k, u_k) \leq 0, \\
& -g^\top \mu_k^{(m)} + (A^{(m)} t(x_k) - b^{(m)})^\top \lambda_k^{(m)} > -s_k^{(m)}, \\
& G^\top \mu_k^{(m)} + R(x_k)^\top {A^{(m)}}^\top \lambda_k^{(m)} = 0, \\
& \|{A^{(m)}}^\top \lambda_k^{(m)}\|_* = 1,\ s_k^{(m)} \geq 0,\ \lambda_k^{(m)} \succeq_{\mathcal{K}^*} 0,\ \mu_k^{(m)} \succeq_{\bar{\mathcal{K}}^*} 0
\end{aligned}\right\} \quad \begin{aligned} & k = 0, \ldots, N, \\ & m = 1, \ldots, M. \end{aligned}
\end{aligned} \tag{18}$$

where $s_k^{(m)} \in \mathbb{R}_+$ is the slack variables associated to the object $\mathbb{O}^{(m)}$ at time step k, and $\kappa \geq 0$ is a weight factor that keeps the slack variable as small as possible. Smoothness of (18) is ensured if $\|\cdot\|$ is the Euclidean distance, and $\mathcal{K}$ and $\bar{\mathcal{K}}$ are either the standard cone or the second-order cone, see also Remark 1.

In the following sections, we illustrate our obstacle avoidance formulation on two applications: a quadcopter path planning problem where the point-mass formulation is used (Section 5), and an automated parking problem where the full-dimensional obstacle avoidance problem formulation is used (Section 6).

5. Example 1: Quadcopter Path Planning

In this section, we illustrate reformulations (10) and (13) on a quadcopter navigation problem, where the quadcopter must find a path from one end of the room to the other end, while avoiding a low-hanging wall and passing through a small window hole, see Figure 1 for an illustration of the setup.

5.1. Environment and Obstacle Modeling

The size of the room is $10.5 \times 10.5 \times 5.5$m, and we see from Figure 1 that the direct path between the start and end position is blocked by two obstacles. The first obstacle, a low-hanging wall, blocks the entire upper part of the room, and can only be passed from below. The second obstacle, another wall, blocks the entire room, but has a small window through which the quadcopter must pass. We approximate the shape of the quadcopter by a (Euclidean) sphere of radius 0.25m. In the framework of (10) and (13), the shape of the quadcopter can be taken into account by requiring a safety distance of $\mathsf{d}_{\min} = 0.25$m.

The first wall, which can only be passed from below, is placed at $X = 2$m, and the passage below is 0.85m high. The second wall is placed at $X = 7$m, and the window is of size 1×1m and is placed in the

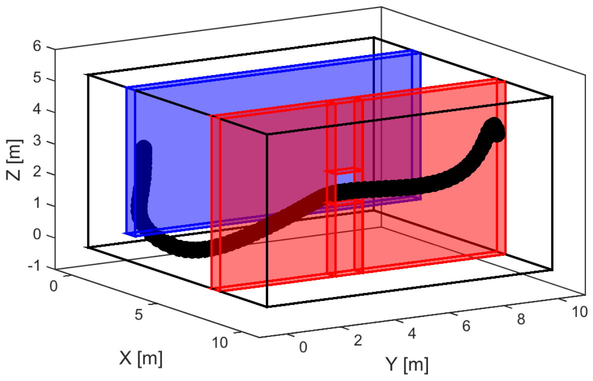

Figure 1: Setup of quadcopter example together with a (locally optimal) point-to-point trajectory. The start position is behind the blue wall at $X = 1$, and the end position in front of red wall at $X = 9$. The quadcopter needs to fly below the blue wall and pass through a window in the red wall, see `https://youtu.be/7WLNJhaHcoQ` for an animation. The black circles illustrate the safety distance $\mathtt{d}_{\min} = 0.25$m which is used to model the shape of the quadcopter.

middle of the room at a height of $Z = 2.5$m. Finally the depth of both walls is 0.5m. This obstacle formation can be formally formulated using five axis-aligned rectangles, where the first obstacle is represented by one such rectangle and the window can be modeled as the union of four rectangles, see Figure 1. The collision avoidance constraints with respect to the four outer walls of the room are achieved by appropriately upper- and lower-bounding the $(X, Y, Z)-$coordinates of the quadcopter.

5.2. Quadcopter Model

We consider the standard quadcopter model as used in [26], which is derived by finding the equation of motion of the center of gravity (CoG). In this model, X, Y, Z denote the position of the CoG in the world frame, and we use the Z-X-Y Euler angles do describe the rotation of the quadcopter, where ϕ is the pitch angle, θ is the roll angle, and ψ is the yaw angle. The rotation matrix that translates from the world to the body frame, which is defined with respect to the CoG, is hence given by

$$R_{WB} = \begin{bmatrix} c_\psi c_\theta - s_\phi s_\psi s_\theta & -c_\phi s_\psi & c_\psi s_\theta + c_\phi s_\psi s_\theta \\ s_\psi c_\theta + s_\phi c_\psi s_\theta & c_\phi c_\psi & s_\psi s_\theta - s_\phi c_\psi c_\theta \\ -c_\phi s_\theta & s_\phi & c_\phi c_\theta \end{bmatrix},$$

where $s_\phi := \sin(\phi)$ and $c_\phi := \cos(\phi)$. The accelerations of the CoG can be derived by considering the sum of the forces produced by the four rotors F_i which point in positive z-direction in the body frame, and the gravity force which acts on the negative z-direction in the world frame, resulting in the following equation of motion,

$$m \begin{bmatrix} \ddot{X} \\ \ddot{Y} \\ \ddot{Z} \end{bmatrix} = \begin{bmatrix} 0 \\ 0 \\ -mg \end{bmatrix} + R_{WB} \begin{bmatrix} 0 \\ 0 \\ \sum_{i=1}^{4} F_i \end{bmatrix} , \tag{19a}$$

where m is the mass of the quadcopter and $\ddot{X}$, $\ddot{Y}$ and $\ddot{Z}$ are the second time derivatives of X, Y and Z, respectively. The attitude dynamics of the quadcopter is derived in the body rates p, q, and r which are related to the Euler angles through the following rotation matrix,

$$\begin{bmatrix} \dot{\phi} \\ \dot{\theta} \\ \dot{\psi} \end{bmatrix} = \begin{bmatrix} c_\theta & 0 & s_\theta \\ s_\theta t_\phi & 1 & -c_\theta t_\phi \\ -s_\theta / c_\phi & 0 & c_\theta / c_\phi \end{bmatrix} \begin{bmatrix} p \\ q \\ r \end{bmatrix} . \tag{19b}$$

The body rates itself are given by the following equation of motion, which is driven by the four rotor forces F_i, as well as the corresponding moments M_i and has the following form,

$$I \begin{bmatrix} \dot{p} \\ \dot{q} \\ \dot{r} \end{bmatrix} = \begin{bmatrix} L(F_2 - F_4) \\ L(F_3 - F_1) \\ M_1 - M_2 + M_3 - M_4 \end{bmatrix} - \begin{bmatrix} p \\ q \\ r \end{bmatrix} \times I \begin{bmatrix} p \\ q \\ r \end{bmatrix} , \tag{19c}$$

where I is the inertia matrix which in our case is diagonal and L is the distance from the CoG to the rotor. The rotor forces and moments depend quadratically on the motor speed ω_i, which are the control inputs and are defined as follows,

$$F_i = k_F \omega_i^2 , \qquad M_i = k_M \omega_i^2 , \tag{19d}$$

where, k_F and k_M are constants depending on the rotor blades. Hence, the state of the quadcopter is $x = [X, Y, Z, \phi, \theta, \psi, \dot{X}, \dot{Y}, \dot{Z}, p, q, r]$ and the inputs are the four rotor speeds $u = [\omega_1, \omega_2, \omega_3, \omega_4]$.

The parameters of the model, as well as the bounds on the inputs, are taken from [27], which corresponds to a quadcopter which weighs 0.5kg and is approximately half a meter in diameter. Furthermore, the angles, velocities and body rates are all limited within bounds, and the dynamics can be brought into the form (1) using a (forward) Euler discretization, such that $x_{k+1} = x_k + T_{\text{opt}} \tilde{f}(x_k, u_k)$, where T_{opt} is the sampling time, and $\tilde{f}(\cdot, \cdot)$ is the continuous-time dynamics that can be obtained from (19a)–(19d).

5.3. Cost function

Our control objective is to fly the quadcopter as fast as possible, while avoiding excessive control inputs. We combine these competing goals as a weighted sum of the form

$$J = q \tau_F + \sum_{k=0}^{N-1} u_k^T R u_k , \tag{20}$$

where τ_F is the final time and $R = R^\top \in \mathbb{R}^{n_u \times n_u} \succeq 0$, and $q \in \mathbb{R} \geq 0$ are weighting factors. In (20), $u_k^T R u_k$ model the minimum input objective, while τ_F represents the minimum time objective. Motivated by [28], we do not directly optimize over τ_F; instead, observing that $\tau_F = N T_{\text{opt}}$, we will treat the discretization time T_{opt} as a decision variable. This motivates the use of the slightly modified cost function $J = q T_{\text{opt}} + \sum_{k=0}^{N-1} u_k^T R u_k$, which will be used in the numerical simulations later on.

Treating T_{opt} as an optimization variable has the additional benefit that the duration of the maneuver does not need to be fixed a priori, allowing us to avoid feasibility issues caused by a too short maneuver length. We point out that this comes at the cost of an additional decision variable T_{opt}, which renders the dynamics “more” non-linear, which can be seen when looking at the Euler discretization in the previous section.

5.4. Choice of Initial Guess

It is well-known that non-convex optimization problems are computationally difficult to solve in general, and that one must content oneself with a *locally optimal solution*, since most NLP-solvers are operate locally. Often times, the solution quality can be influenced by the choice of the initial guess. Ideally this initial guess satisfies all constraints including the obstacle avoidance and system constraints. For the quadcopter application we have found that a (X, Y, Z)-path that avoids all obstacles (but not necessarily satisfies the system dynamics) results in a good performance, while the other variables are initialized with zero. A feasible (X, Y, Z)-path is constructed using ordered waypoints which are connected with lines and are chosen such that the lines do not intersect with the obstacles. In our set-up this results in a path consisting of five straight segments connecting the starting and finishing point while avoiding all the obstacles, see Figure 2.

5.5. Simulation Results

To verify the performance and robustness of our approach, we considered 36 path planning scenarios, each starting and ending in a hovering points. The starting point is always located at $X = 1$, $Y = 1$, $Z = 3$m, and the finishing point is always located behind the wall with the window at $X = 9$m, but with varying Y and Z coordinates. The final positions are generated by gridding the (Y, Z) space with nine points in the Y direction and four points in the Z direction as shown in Figure 3. We tested both the distance formulation (10) as well as the signed distance formulation with soft constraints (13). We use a horizon of $N = 80$ and limit the sampling time T_{opt} to lie between 0.125s and 0.375s. The optimization problems are implemented with the modeling toolbox JuMP in the programming language Julia [29], and solved using the general purpose nonlinear solver IPOPT [22]. The problems are solved on a MacBook Pro with an i7 processor clocked at 2.4 GHz.

Figure 3 shows the computation time as a function of the finishing position, where a circle implies that a (locally optimal) solution was found successfully, see Figure 1 for such a trajectory. Despite having more

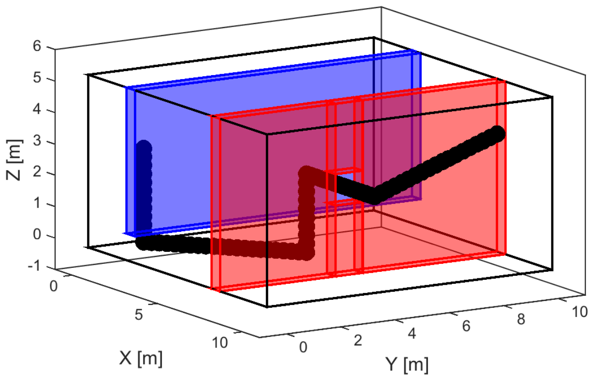

Figure 2: The chosen warm start trajectory for the quadcopter is shown. Notice that this trajectory avoids obstacles but does not satisfy the dynamic constraints of the quadcopter, which will be corrected by the optimization algorithm. The black tubes is the safety distance $\mathsf{d}_{\min}$ which is used to model the shape of the quadcopter.

decision variables, we observe from Figure 3 that the signed-distance approach (right) is solved not only slightly faster overall, but also has fewer outliers in terms of computation time. Furthermore, notice that both approaches are able to compute all paths but one. Interestingly, we observe that the unsuccessful scenarios, as well as computation times of the two approaches, are not correlated; in other words, a “difficult” scenario for the distance approach might be “easy” for the signed distance approach, and vice versa. In practice, this implies that to obtain feasible trajectories as fast as possible, the navigation problem should be solved with both obstacle avoidance formulations, and the first solution should be taken. For our problem setup, this would result in a worst case computation time of 22.0s.

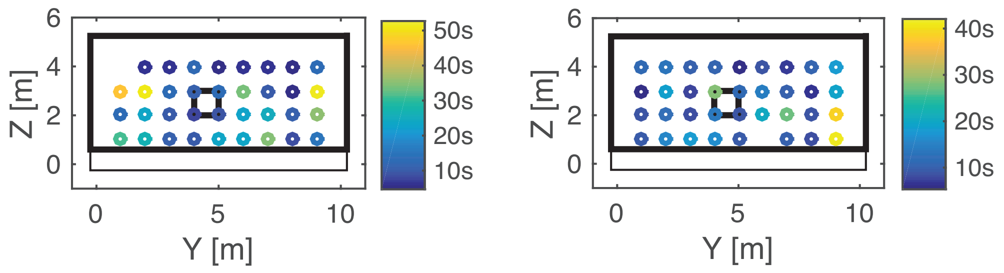

Figure 3: Solution time for quadcopter trajectory planning with distance approach (left) and signed-distance approach (right). Median computation time for distance approach is 12.2s, while median computation time for signed-distance is 10.4s. One scenario in each case could not be obtained.

6. Example 2: Autonomous Parking

As a second application for our collision avoidance formulation, we consider the autonomous parking problem of self-driving cars. In contrast to the quadcopter case, modeling a car as a point-mass and then conservatively approximating its shape through a ball can be very conservative and prevent a car finding a feasible trajectory, especially in tight environments. In this section, we model the car as a rectangle, and then employ the full-dimensional approach of Section 4 to the parking problem. Two scenarios are considered: backward parking (Figure 4) and parallel parking (Figure 5).

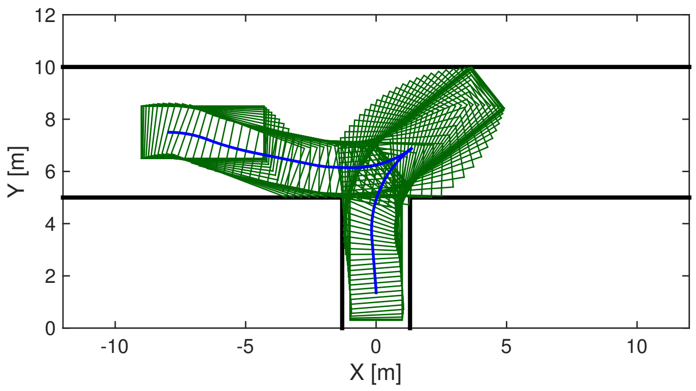

Figure 4: Backward parking maneuver. The controlled vehicle is shown in green at every time step. Vehicle starts facing to the right, and ends facing upwards, see `https://youtu.be/2NcfVE52q1U` for an animation.

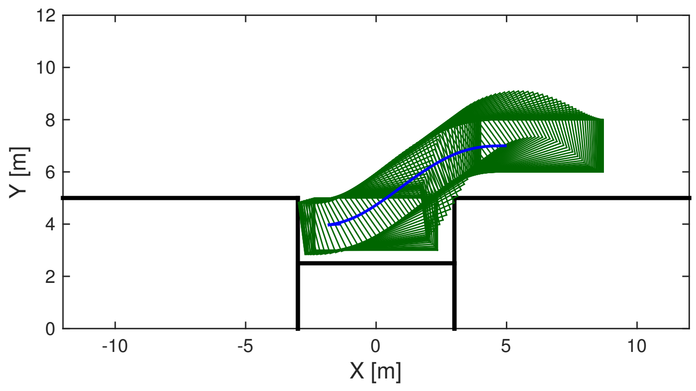

Figure 5: Parallel parking maneuver. The controlled vehicle is shown in green at every time step. Vehicle starts facing to the right, and ends facing to the right, see `https://youtu.be/igDkznOzPGw` for an animation.

6.1. Environment and Obstacle Modeling

For the backwards parking scenario, the parking spot is assumed 2.6m wide and 5.2m long. The width of the road, where the car can maneuver in, is 5m, see Figure 4 for an illustration. For the parallel parking scenario, the parking spot is 2.5m deep and 6m long, and the space to maneuver is 7m wide (Figure 5). Note that both parking situations can be described by 3 axis aligned boxes serving as obstacles. Finally, in both cases, the controlled vehicle is modeled as a rectangle of size 4.7×2m, whose orientation is determined by the car's yaw angle.

6.2. System Dynamics and Cost Function

The car is described by the classical kinematic bicycle model, which is well-suited for velocities used in typical parking scenarios. The states (X, Y) correspond to the center of the rear axes, while φ is the yaw angle with respect to the X-axis, and v is the velocity with respect to the rear axes. The inputs are the steering angle δ and the acceleration a. Hence, the continuous-time dynamics of the car is given by

$$\begin{aligned}
\dot{X} &= v\cos(\varphi)\,, \\
\dot{Y} &= v\sin(\varphi)\,, \\
\dot{\varphi} &= \frac{v\tan(\delta)}{L}\,, \\
\dot{v} &= a\,,
\end{aligned}$$

where $L = 2.7$m is the wheel base of the car. The steering angle is limited between ± 0.6rad (approximately 34 degrees) and acceleration between ± 1m/s^2. We limit the car's velocity to lie between -1 and 2m/s. Similar as in the quadcopter case, the continuous-time dynamics are discretized using a forward Euler scheme. Finally, the same cost function as in the quadcopter is used, i.e., a weighted sum between the discretization-time and control effort is considered.

6.3. Initial Guess

In contrast to the quadcopter case, finding meaningful way points as good initial guesses is more challenging because the yaw angle of the car needs to be considered when constructing an initial guess. Therefore, we propose the use of an alternative approach, where we first solve a point-to-point trajectory planning problem without any obstacles, and then use this trajectory as a initial guess to warm start the full optimization problem, see Figures 6 and 7 for the warm start trajectories associated to the trajectories in Figures 4 and 5. While this often results in a reasonable initial guess, it does not guarantee success at all times as we will see next.

6.4. Simulation Results

To evaluate the performance of the collision avoidance formulations (15) and (18), we study the backward and parallel trajectory planning problem. For both cases, we consider different starting positions but one fixed end position at $X = 0$, and investigate the performance and success rate of each method. The starting

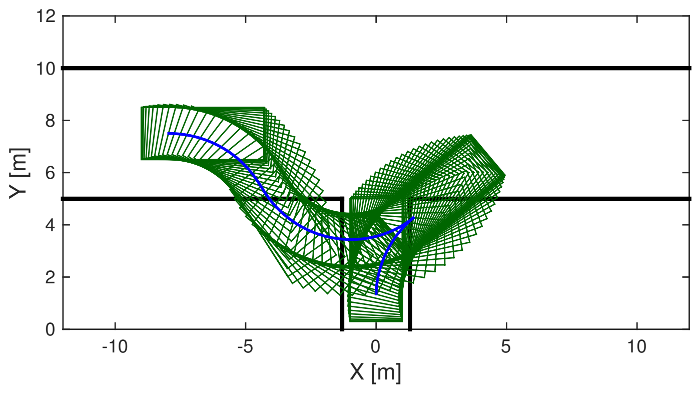

Figure 6: Initial guess for the backward parking maneuver, with the controlled vehicle shown in green at every time step.

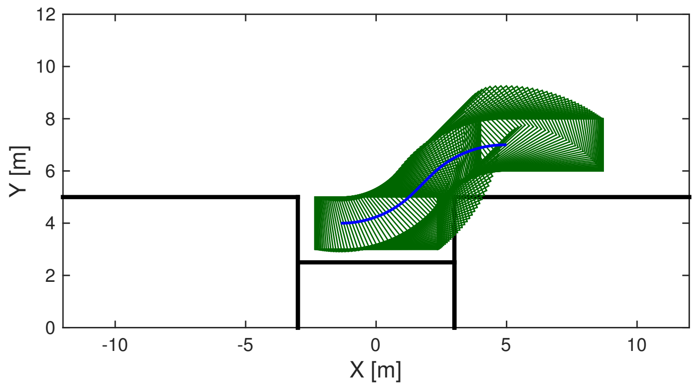

Figure 7: Initial guess 2 for the parallel parking maneuver, with the controlled vehicle shown in green at every time step.

positions are generated by gridding the maneuvering space within $X \in [-10, 10]$ and $Y \in [5, 10]$, with eleven points in the X direction and 5 points in Y direction, see Figure 8. The orientation for all the starting points is $\varphi = 0$, resulting in a total of 105 starting points. For the specific implementation, we use a horizon of $N = 80$ and a variable sampling time $T_{\text{opt}} \in [0.15, 0.6]$. The optimization problems are again implemented with the modeling toolbox JuMP in the programming Julia [29], and IPOPT [22] is used as the NLP solver. The problems are solved on a MacBook Pro with a i7 processor clocked at 2.4 GHz.

We begin by considering the backward parking case, where one specific maneuver is illustrated in Figure 4. The computation times for the distance and the signed distance approaches are shown in Figure 8, for all 105 initial conditions. In contrast to the quadcopter example, the distance approach is faster than the signed-distance approach, with a median computation time of 2.1s compared to 7.0s. Furthermore, notice that both approaches are able to find trajectories for all considered initial conditions. Interestingly, we see that there are no obvious connections between starting positions and solution times.

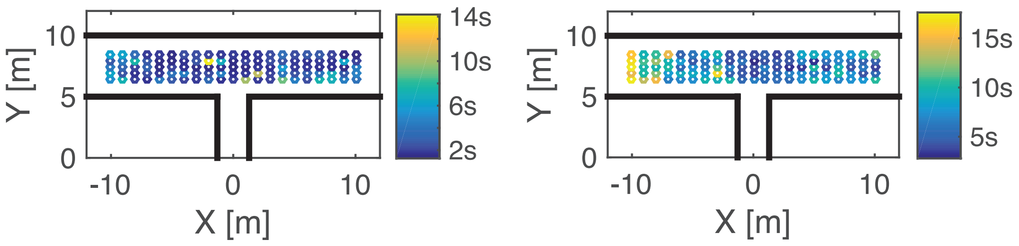

Figure 8: Solution time for backwards parking with distance approach (left) and signed-distance approach (right). It can be seen that the signed-distance approach is computationally more demanding than the distance approach.

For the parallel parking case, Figure 5 shows one parking instance, while Figure 9 depicts the computation time for different initial conditions. Compared to the backward parking case, we see that neither approach (i.e., distance and signed-distance) has a 100% success rate. Specifically, we see that starting points with $X \in [-10, -5]$ are difficult for the distance approach, where the computation times are high and success rates are low. We believe that this effect can be attributed to the choice of our initial guess, since the optimal path with and without obstacles can be dramatically different for these starting points, see Figure 10 for such a scenario. Finally, we point out that while the signed-distance approach is computationally more challenging on average, it shows better performance than the distance approach in terms of success rates, a phenomena that requires further investigation.

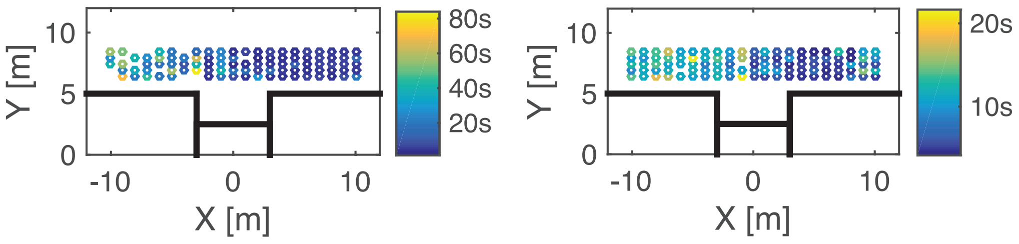

Figure 9: Solution time for parallel parking with distance approach (left) and signed-distance approach (right). It can be seen that, overall, the signed-distance approach is more robust and computationally demanding than the distance approach. Median computation time is 6.4s for distance approach, and 9.7s for signed-distance approach.

7. Conclusion

In this paper, we presented smooth reformulations for collision avoidance constraints for problems where the controlled object and the obstacle can be represented as the finite union of convex sets. We have

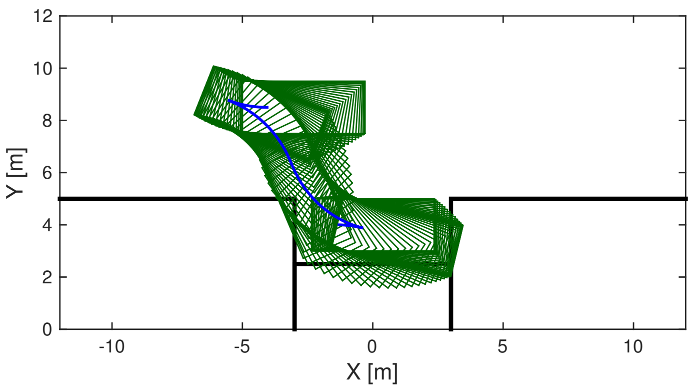

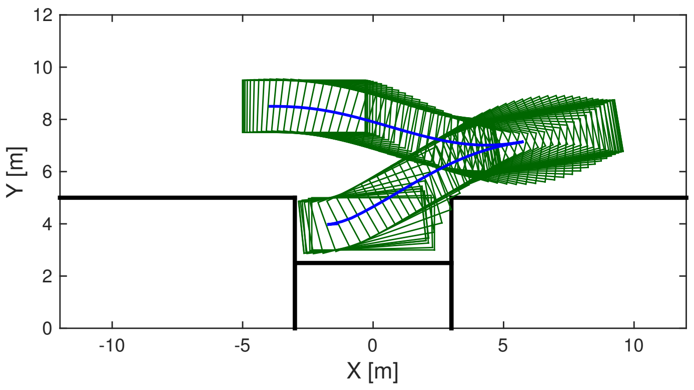

Figure 10: A parallel parking scenario where the warm-start trajectory (top) significantly deviates from the final trajectory (bottom). The controlled vehicle shown in green at every time step. An animation of the collision-free trajectory can be found at `https://youtu.be/t5HOGLQiAu8`.

shown that non-differentiable polytopic obstacle constraints can be dealt with via dualization techniques to preserve differentiability, allowing the use of gradient- and Hessian-based optimization methods. The presented reformulation techniques are exact and non-conservative, and apply equally to point-mass and full-dimensional controlled vehicles. Furthermore, in case collision-free trajectories cannot be generated, our framework allows us to find least-intrusive trajectories, measured in terms of penetration.

Our numerical studies, performed on a quadcopter trajectory planning and car parking example, indicate that the signed-distance reformulation is numerically more stable than the simpler distance reformulation, although the latter can yield lower computation times. Furthermore, we have seen that the performance of the numerical algorithms to solve the non-convex optimization problems depends on the choice of the initial guess. Current research focuses on the appropriate choice of initial guesses, as well as methods for speeding up computation time.

Appendix A. Proof of Proposition 2

We need the following auxiliary result:

Lemma 1. *Let $\mathbb{C} \subset \mathbb{R}^n$ be a compact convex set and let $\mathcal{H}(z) := \{x \colon z^\top x \leq \max_{y\in\mathbb{C}} y^\top z\}$. Then $\partial\mathcal{H}(z)$ is a supporting hyperplane of $\mathbb{C}$, and*

$$\mathbb{C} = \bigcap_{z\colon \|z\|=1} \mathcal{H}(z), \tag{A.1}$$

for any norm $\|\cdot\|$.

Proof of Proposition 2

It is easy to see that $\text{pen}(\mathbb{E}(x), \mathbb{O}) = \text{dist}(\mathbb{E}(x), \mathbb{O}^{\complement})$, where $\mathbb{C}^{\complement} \subset \mathbb{R}^n$ denotes the complement of the set $\mathbb{C}$. Using this definition and recalling that $\mathbb{E}(x)$ is a point-mass, it follows from Lemma 1 that $\text{pen}(\mathbb{E}(x), \mathbb{O}) = \inf_{\{z\colon \|z\|_*=1\}} \text{dist}(\mathbb{E}(x), \partial\mathcal{H}(z))$, where we exploited the fact that (A.1) holds for any norm, and hence also the dual norm $\|\cdot\|_*$. Furthermore, it can be shown that $\text{dist}(\mathbb{E}(x), \partial\mathcal{H}(z)) = \max_{y\in\mathbb{C}}\{y^\top z\} - z^\top\mathbb{E}(x)$, which allows us to express the penetration function as $\text{pen}(\mathbb{E}(x), \mathbb{O}) = \inf_{\{z\colon \|z\|_*=1\}} \left\{\max_{y\in\mathbb{C}}\{y^\top z\} - z^\top\mathbb{E}(x)\right\}$. So see that the min-max problem implies (11), we use strong duality of convex optimization to reformulate the inner maximization problem as $\max_{y\in\mathbb{C}}\{y^\top z\} = \min_\lambda\{b^\top\lambda\colon A^\top\lambda = z,\ \lambda \succeq_{\mathcal{K}^*} 0\}$. Hence, $\text{pen}(\mathbb{E}(x), \mathbb{O}) = \inf_{z,\lambda}\{b^\top\lambda - z^\top\mathbb{E}(x)\colon \|z\|_* = 1,\ A^\top\lambda = z,\ \lambda \succeq_{\mathcal{K}^*} 0\} = \inf_\lambda\{(b - A\mathbb{E}(x))^\top\lambda\colon \|A^\top\lambda\|_* = 1,\ \lambda \succeq_{\mathcal{K}^*} 0\}$. Finally, we have $\text{pen}(\mathbb{E}(x), \mathbb{O}) < \mathsf{p}_{\max} \Leftrightarrow \inf_\lambda\{(b - A\mathbb{E}(x))^\top\lambda\colon \|A^\top\lambda\|_* = 1,\ \lambda \succeq_{\mathcal{K}^*} 0\} < \mathsf{p}_{\max} \Leftrightarrow \lambda \succeq_{\mathcal{K}^*} 0\colon (b - A\,\mathbb{E}(x))^\top\lambda < \mathsf{p}_{\max}$, which concludes the proof.

References

[1] A. Richards and J. P. How. Aircraft trajectory planning with collision avoidance using mixed integer linear programming. In *Proceedings of the 2002 American Control Conference (IEEE Cat. No.CH37301)*, volume 3, pages 1936–1941, May 2002.

[2] F. Borrelli, T. Keviczky, and G. J. Balas. Collision-free uav formation flight using decentralized optimization and invariant sets. In *2004 43rd IEEE Conference on Decision and Control (CDC) (IEEE Cat. No.04CH37601)*, volume 1, pages 1099–1104 Vol.1, Dec 2004.

[3] M. Diehl, H.G. Bock, H. Diedam, and P.-B. Wieber. *Fast Direct Multiple Shooting Algorithms for Optimal Robot Control*, pages 65–93. Springer Berlin Heidelberg, Berlin, Heidelberg, 2006.

[4] L. Blackmore and B. Williams. Optimal manipulator path planning with obstacles using disjunctive programming. In *2006 American Control Conference*, pages 3 pp.–, June 2006.

[5] Yiqi Gao, Theresa Lin, Francesco Borrelli, Eric Tseng, and Davor Hrovat. Predictive control of autonomous ground vehicles with obstacle avoidance on slippery roads. In *ASME Dynamic Systems and Control Conference*, 2010.

[6] R. Patel and P. J. Goulart. Trajectory generation for aircraft avoidance maneuvers using online optimization. *AIAA Journal of Guidance, Control and Dynamics*, 34(1):218–230, 2011.

[7] L. Blackmore, M. Ono, and B. C. Williams. Chance-constrained optimal path planning with obstacles. *IEEE Transactions on Robotics*, 27(6):1080–1094, Dec 2011.

[8] Salmah, Sutrisno, E. Joelianto, A. Budiyono, I. E. Wijayanti, and N. Y. Megawati. Model predictive control for obstacle avoidance as hybrid systems of small scale helicopter. In *2013 3rd International Conference on Instrumentation Control and Automation (ICA)*, pages 127–132, Aug 2013.

[9] John Schulman, Yan Duan, Jonathan Ho, Alex Lee, Ibrahim Awwal, Henry Bradlow, Jia Pan, Sachin Patil, Ken Goldberg, and Pieter Abbeel. Motion planning with sequential convex optimization and convex collision checking. *The International Journal of Robotics Research*, 33(9):1251–1270, 2014.

[10] A. Liniger, A. Domahidi, and M. Morari. Optimization-based autonomous racing of 1:43 scale RC cars. *Optimal Control Applications and Methods*, 36(5):628–647, 2015.

[11] U. Rosolia, A. Carvalho, and F. Borrelli. Autonomous racing using learning model predictive control. In *American Control Conference (ACC), 2017*. IEEE, 2017.

[12] J. Funke, M. Brown, S. M. Erlien, and J. C. Gerdes. Collision avoidance and stabilization for autonomous vehicles in emergency scenarios. *IEEE Transactions on Control Systems Technology*, 25(4):1204–1216, July 2017.

[13] Brian Paden, Michal Cáp, Sze Zheng Yong, Dmitry S. Yershov, and Emilio Frazzoli. A survey of motion planning and control techniques for self-driving urban vehicles. *IEEE Transactions on Intelligent Vehicles*, 1:33–55, 2016.

[14] Christos Katrakazas, Mohammed Quddus, Wen-Hua Chen, and Lipika Deka. Real-time motion planning methods for autonomous on-road driving: State-of-the-art and future research directions. *Transportation Research Part C: Emerging Technologies*, 60:416 – 442, 2015.

[15] I. E. Grossmann. Review of Nonlinear Mixed-Integer and Disjunctive Programming Techniques. *Optimization and Engineering*, 3(3):227–252, 2002.

[16] M. Klauco. Notes on obstacle avoidance and mpc, 2016.

[17] Ugo Rosolia, Stijn De Bruyne, and Andrew G Alleyne. Autonomous vehicle control: A nonconvex approach for obstacle avoidance. *IEEE Transactions on Control Systems Technology*, 25(2):469–484, 2017.

[18] Tobias Nägeli, Javier Alonso-Mora, Alexander Domahidi, Daniela Rus, and Otmar Hilliges. Real-time motion planning for aerial videography with dynamic obstacle avoidance and viewpoint optimization. *IEEE Robotics and Automation Letters*, 2(3):1696–1703, 2017.

[19] Bai Li and Zhijiang Shao. A unified motion planning method for parking an autonomous vehicle in the presence of irregularly placed obstacles. *Knowledge-Based Systems*, 86:11 – 20, 2015.

[20] T.R. Rockafellar. *Convex Analysis*. Princeton University Press, 1970.

[21] S. Boyd and L. Vandenberghe. *Convex Optimization*. Cambridge University Press, 2004.

[22] Andreas Wächter and Lorenz T. Biegler. On the implementation of an interior-point filter line-search algorithm for large-scale nonlinear programming. *Mathematical Programming*, 106(1):25–57, Mar 2006.

[23] S. Cameron and R. Culley. Determining the minimum translational distance between two convex polyhedra. In *International Conference on Robotics and Automation*, volume 3, pages 591–596, Apr 1986.

[24] David Dobkin, John Hershberger, David Kirkpatrick, and Subhash Suri. Computing the intersection-depth of polyhedra. *Algorithmica*, 9(6):518–533, Jun 1993.

[25] F. Borrelli, A. Bemporad, and M. Morari. *Predictive control for linear and hybrid systems*. Cambridge University Press, 2017.

[26] Daniel Mellinger, Nathan Michael, and Vijay Kumar. Trajectory generation and control for precise aggressive maneuvers with quadrotors. *The International Journal of Robotics Research*, 31(5):664–674, 2012.

[27] Daniel Warren Mellinger. Trajectory generation and control for quadrotors. 2012.

[28] Fariba Fahroo and I Micheal Ross. Direct trajectory optimization by a chebyshev pseudospectral method. In *American Control Conference, 2000. Proceedings of the 2000*, volume 6, pages 3860–3864. IEEE, 2000.

[29] Iain Dunning, Joey Huchette, and Miles Lubin. Jump: A modeling language for mathematical optimization. *SIAM*

Review, 59(2):295–320, 2017.